Journal of Solar Energy Research (JSER)

Journal homepage: jser.ut.ac.ir

Energy, Exergy and Economic Analysis of Solar Air Heaters with Different Roughness Geometries

Milad Shadi[a], Somayeh Davoodabadi Farahani[b], Abolfazl Hajizadeh Aghdam[c*]

[a,b,c] *Department of Mechanical Engineering, Arak University of Technology, Arak 38181-46763, Iran*

Abstract

Artificially roughened surface is a common method to enhance the heat transfer in a flow passage. Energy, exergy and economic analysis of solar air heaters with different roughness geometries have been done. To improve the performance of the solar collector, 4 different types of roughness on the absorber plate have been used. The mathematical model has been validated with analytical and experimental results available in the literature with acceptable deviation. On the basis of numerical calculations, it has been concluded that roughened surface improves energy and exergy efficiency of solar air heater by 14 % and 1%, respectively. Further it was found that the most efficient roughness is Discrete V Rib and the least expensive roughness is U-Shape turbulator. NSGA II and TOPSIS algorithms used to select the best roughness geometry.

Keywords: Solar Air Heater; Exergy Analysis; Annual Cost; Roughness; NSGA II

1. Introduction

The flat-plate solar air heaters (SAH) are extensively employed in low temperature energy applications such as space heating, drying of agricultural products and various industrial applications. Heat transfer from the absorber of solar air heater to air is low due to a presence of viscous/laminar sublayer in turbulent boundary layer. Heat transfer rate in a viscous sublayer is adversely affected due to lower thermal conductivity and relatively low velocity of air [1]. One of the methods to overcome this problem is provision of the artificial rib roughness on the underside of the absorber of solar air heater to restrict development of the viscous sublayer and thermal boundary layer. The artificial rib roughness on a heat transfer surface in the form of projections mainly creates turbulence near the wall, breaks the viscous sublayer and thus enhances the heat transfer coefficient with a minimum pressure loss penalty. The ribroughness geometries such as transverse [2,3], inclined [4], V-up [5] and V-down [4] are some common reported geometries to enhance the thermal performance of solar air heaters. These studies have shown that V-down ribs perform better than V-up ribs. Further, V-up ribs perform better than angled and transverse ribs. It has been reported that discretization of rib roughness results in even higher thermal performance due to flow through the gap [4,6,7]. However, it is reported that the artificial rib roughness results in simultaneous enhancement in frictional losses leading to more power requirement for fluid to flow through the duct. Hans et al. [8] have given detailed review of large number of ribroughness geometries investigated for solar air heaters. The studies have shown that dimensionless rib-roughness parameters such as relative roughness pitch, relative roughness height, angle of attack, etc. have an important

*corresponding author Email address:a.hajizadeh@arakut.ac.ir

Table.1 Correlations of heat transfer and friction factors for SAH with different roughness elements on top side of absorber plate

No	Rib	Shape	Correlation	Roughness Variable
1	Multi V Shape	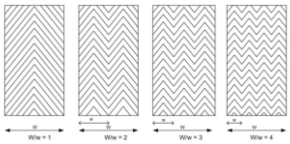	$f=\left(4.47\times10^{-4}\right)(\mathrm{Re})^{-0.3188}\left(\frac{e}{D_h}\right)^{0.73}\left(\frac{p}{e}\right)^{8.9}\left(\frac{W}{w}\right)^{0.22}\left(\frac{\alpha}{90}\right)^{-0.39}e^{-0.52\left(\ln\left(\frac{\alpha}{90}\right)\right)^2}e^{-2.133\left(\ln\left(\frac{p}{e}\right)\right)^2}$ $Nu=\left(3.35\times10^{-5}\right)(\mathrm{Re})^{0.92}\left(\frac{e}{D_h}\right)^{0.77}\left(\frac{p}{e}\right)^{8.54}\left(\frac{W}{w}\right)^{0.43}\left(\frac{\alpha}{90}\right)^{-0.49}e^{-0.61\left(\ln\left(\frac{\alpha}{90}\right)\right)^2}e^{-2.0407\left(\ln\left(\frac{p}{e}\right)\right)^2}e^{-0.1177\left(\ln\left(\frac{W}{w}\right)\right)^2}$	$0.019\le\frac{e}{D_h}\le0.043$ $6\le\frac{p}{e}\le12$ $1\le\frac{W}{w}\le10$ $30\le\alpha\le75$
2	U Shape Turbulator	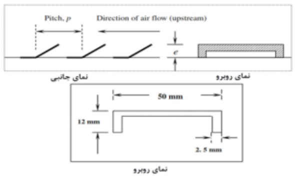	$f=1.2134(\mathrm{Re})^{-0.2076}\left(\frac{e}{D_h}\right)^{0.3285}\left(\frac{p}{e}\right)^{-0.4259}$ $Nu=0.5429(\mathrm{Re})^{0.7054}\left(\frac{e}{D_h}\right)^{0.3619}\left(\frac{p}{e}\right)^{-0.1592}$	$0.0186\le\frac{e}{D_h}\le0.0398$ $6.66\le\frac{p}{e}\le57.14$
3	Winglet and Wavy Grooves	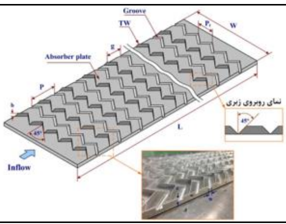	$f=18.39(\mathrm{Re})^{-0.056}(B_R)^{1.239}(P_R)^{-0.821}$ $Nu=0.48(\mathrm{Re})^{0.771}(\mathrm{Pr})^{0.4}(B_R)^{0.538}(P_R)^{-0.411}$	$0.12\le B_R\le0.28$ $6.66\le P_R\le57.14$ $4\le\frac{p}{e}\le12$
4	Discrete V Rib	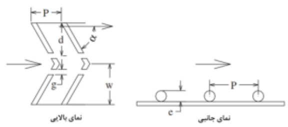	$f=\left(4.13\times10^{-2}\right)(\mathrm{Re})^{-0.126}\left(\frac{e}{D_h}\right)^{0.7}\left(\frac{g}{e}\right)^{0.031}\left(\frac{p}{e}\right)^{2.74}\left(\frac{d}{w}\right)^{-0.058}\left(\frac{\alpha}{60}\right)^{-0.034}e^{-0.93\left(\ln\left(\frac{\alpha}{60}\right)\right)^2}e^{-0.658\left(\ln\left(\frac{p}{e}\right)\right)^2}e^{-0.58\left(\ln\left(\frac{d}{w}\right)\right)^2}e^{-0.21\left(\ln\left(\frac{g}{e}\right)\right)^2}$ $Nu=\left(2.36\times10^{-3}\right)(\mathrm{Re})^{0.9}\left(\frac{e}{D_h}\right)^{0.47}\left(\frac{g}{e}\right)^{-0.014}\left(\frac{p}{e}\right)^{3.5}\left(\frac{d}{w}\right)^{-0.043}\left(\frac{\alpha}{60}\right)^{-0.023}e^{-0.72\left(\ln\left(\frac{\alpha}{60}\right)\right)^2}e^{-0.84\left(\ln\left(\frac{p}{e}\right)\right)^2}e^{-0.05\left(\ln\left(\frac{d}{w}\right)\right)^2}e^{-0.15\left(\ln\left(\frac{g}{e}\right)\right)^2}$	$0.015\le\frac{e}{D_h}\le0.043$ $0.5\le\frac{g}{e}\le2$ $0.2\le\frac{d}{w}\le0.8$ $30\le\alpha\le70$ $4\le\frac{p}{e}\le12$

influence on heat transfer and friction characteristics of the rib roughened duct. Nature of discretization of ribs also influences the performance of the rib roughened duct.

As the artificial rib roughness results in heat transfer enhancement with simultaneous increase in friction power penalty, it is useful to know in advance which combination of the artificial ribroughness parameters will lead to an improvement in overall performance of a solar air heater. In addition, it is important to know the improvement quantitatively.

Various methods for predicting the performance of solar air heaters have been reported. Esen et al. [9,10] determined performance of a double flow solar air heaters using least-squares support vector machines, artificial neural network and wavelet neural network approaches, and compared the results with the experimental results reported by Ozgen et al. [11]. Gupta [12], Saini [13] and Karwa et al. [14,15] determined performance of a roughened solar air heater using effective efficiency criterion. Second law of thermodynamics based exergy analysis incorporates quality of useful energy output and frictional losses. The exergy concept based on the second law of thermodynamics provides an analytical framework for system performance evaluation. The exergy is the maximum work potential that can be obtained from a form of energy [16]. The exergy analysis yields useful results because it deals with the irreversibility minimization or maximum exergy delivery. The exergy analysis has proved to be a powerful tool in the thermodynamic analysis of energy systems [17]. The second law based analysis of rib roughened solar air heaters has been reported by Layek et al. [18] and Gupta and Kaushik [19,20]. Layek et al. [18] studied numerically the entropy generation in the duct of a solar air heater having the transverse chamfered rib-groove roughness. Ribroughness

parameters for the minimum entropy generation are found. Gupta and Kaushik [19] did the energy, effective and exergetic efficiency based performance evaluation of a solar air heater roughened with different rib-roughness geometries. It was reported that not a single geometry gives best exergetic performance for the whole range of Reynolds number. Gupta and Kaushik [20] reported the exergetic efficiency as suitable criterion for performance evaluation of the expended metal mesh roughened solar air heater. Suitable design parameters of the expended metal mesh were determined. The second law based analysis has also been reported for flat-plate solar air heater [21,22], corrugated absorber solar air heater [23], Raschig rings packed bed solar air heater [24], passively augmentated absorber solar air heater [25], double flow solar air heater [26], indirect solar cabinet dryer [27], thin layer drying of mulberry in a forced solar dryer [28], solar drying process of pistachio [29] and solar-assisted heat pump [30,31].

In this investigation, multi-objective optimization of solar air heater roughened with different ribs have been carried out to maximize the thermal and exergetic efficiency and minimize annual cost of solar air heater. For this purpose we choose four different ribs that have a better performance in solar air heaters. Discrete V-down rib [32], winglet and wavy groove [33], Multi V rib [34] and U-shape turbulator [35] used as rib-roughness. Experimental investigations were carried by the authors to generate heat transfer and friction factor data pertinent to heating of air in a rectangular duct. (detailed experimentation, quantitative results and correlations are discussed in earlier published paper [33-36]). For this purpose we use NSGA II algorithm to find best data combination in optimization. This method give us 200 combination of variables. To choose the best one we use TOPSIS algorithm. All of algorithm and optimization equation has been resolved in MATLAB 16.

As shown in Table 1 , In this article we used 4 geometry for rib-roughness that worked best.

2. Materials and Methods

2.1. Energy and Exergy Analysis

The thermal performance of a solar air heater can be predicted on the basis of detailed consideration of heat transfer processes in the system. Using the correlations for heat transfer coefficient for flat plate solar air heater and the performance parameters (overall heat loss coefficient, heat removal factor etc.) can be evaluated. For this purpose, a step by step procedure has to be followed. In order to compute the top loss coefficient and heat removal factor plate temperatures are assumed and an iterative process is followed. Various steps involved in the iterative process have been explained below [37]. A computer program based on the proposed optimization in the next section of these calculations has been developed in MATLAB 16 software.

Step 1: An initial estimate for the mean absorber plate temperature T_o, is made by using the approximation $T_o=T_a+5$.

Step 2: Using this plate temperature, top loss coefficient, U_T and then overall loss coefficient, U_L are computed using the following equations. The top loss coefficient U_T can be computed using the relationship proposed by Klein [38] as given below:

$$U_L = U_t + \frac{k_i}{t} \tag{1}$$

$$U_t = \left[\frac{N}{\left(\frac{C}{T_p}\right)\left[\frac{T_p - T_a}{N+f}\right]^e} + \frac{1}{h_w} \right]^{-1} + \frac{\left(\sigma\left(T_p^2 + T_a\right)\left(T_p + T_a\right)\right)}{\left[\varepsilon_p + 0.00591 N h_w\right]^{-1} + \left[\frac{2N + f - 1 + 0.133\varepsilon_p}{\varepsilon_p}\right] + N} \tag{2}$$

$$f = \left(1 + 0.089 h_w - 0.1166 h_w \varepsilon_p\right)\left(1 + 0.07866 N\right) \tag{3}$$

$$C = 520\left(1 - 0.000051\beta^2\right) \tag{4}$$

$$e = 0.43\left(1 - \frac{100}{T_p}\right) \tag{5}$$

Step 3: By using this estimated loss coefficient U_L, the efficiency factor F_0 and heat removal factor F0 are computed using the following equations. The heat removal factor, F_0 is given by

$$F_0 = \frac{\dot{m}C_p}{U_L A_p}\left[1-\exp\left(\frac{U_L A_p F'}{\dot{m}C_p}\right)\right] \tag{6}$$

Where F' is

$$F' = \frac{h}{U_L + h} \tag{7}$$

The heat transfer coefficient h can be determined from the correlation developed for rib-roughness.

Net thermal energy gain is then computed using the following equation.

$$Q_u = F_0 A_p \left[I(\tau\alpha) - U_L (T_o - T_i) \right] \tag{8}$$

The temperature rise is computed using the equation given below

$$(T_o - T_i) = \frac{Q_u}{\dot{m}C_p} \tag{9}$$

Step 4: These estimates for heat removal factor F_0, loss coefficient U_L, heat energy gain qu, and temperature rise $(T_o - T_i)$ are then used in the following equation to compute the new mean plate temperature.

$$T_p = T_a + F_0 I(\tau\alpha)\left[\frac{1-F_0}{F_0 U_L} + \frac{(T_o - T_i)}{I(\tau\alpha)}\right] \tag{10}$$

Step 5: This new mean plate temperature is compared with the previous value and the difference decides the further course of calculations. If difference is within acceptable limits, the process is terminated w hile if the difference is outside the tolerance limits the calculated value of T_p is used as revised value.

Step 6: Using this revised value of mean plate temperature the above steps (1–5) are repeated till new and old values of mean plate temperature agree within specified limits.

Step 7: When the correct plate temperature has been determined from this iterative procedure, the thermal performance of solar air heater is calculated by using the following expression.

$$\eta_{th} = F_0\left[(\tau\alpha) - U_L\left(\frac{T_o - T_i}{I}\right)\right] \tag{11}$$

The air properties can be calculated by the following equations [39] :

$$\rho = \begin{cases} -2.44\times10^{-2}T + 5.9958, & 100K \le T < 150K \\ 345.57(T-2.6884)^{-1}, & 150K \le T \le 3000K \end{cases} \tag{12}$$

$$\begin{aligned}\mu &= 2.5914\times10^{-15}T^3 - 1.4346\times10^{-11}T^2 \\ &+ 5.0523\times10^{-8}T + 4.1130\times10^{-6}\end{aligned} \tag{13}$$

$$\begin{aligned}C_p &= 1.3864\times10^{-13}T^4 - 6.4747\times10^{-10}T^3 \\ &+ 1.0234\times10^{-6}T^2 - 4.3282\times10^{-4}T + 1.0613\end{aligned} \tag{14}$$

$$\begin{aligned}k_a &= 1.5797\times10^{-17}T^5 + 9.46\times10^{-14}T^4 \\ &+ 2.2012\times10^{-10}T^3 - 2.3758\times10^{-7}T^2 \\ &+ 1.7082\times10^{-4}T - 7.488\times10^{-3}\end{aligned} \tag{15}$$

$$\begin{aligned}\mathrm{Pr} &= 1.0677\times10^{-23}T^7 - 7.6511\times10^{-20}T^6 \\ &+ 1.0395\times10^{-16}T^5 + 4.6851\times10^{-13}T^4 \\ &- 1.7698\times10^{-9}T^3 + 2.226\times10^{-6}T^2 \\ &- 1.1262\times10^{-3}T + 0.88353\end{aligned} \tag{16}$$

The characteristic dimension or equivalent diameter of duct is given by:

$$D_h = 2ab/(a+b) \tag{17}$$

The pressure loss ΔP through the air heater duct, is [40] :

$$\Delta P = \frac{2fcv^2\rho}{D_h} \tag{18}$$

According to Petela's theory, the exact exergy income by solar radiation for a typical collector with surface area of A_p becomes $IA_p\eta_p$.

η_p Is Petela's efficiency of converting radiation energy into work [41] :

$$\eta_P = 1 - \frac{4}{3}\left(\frac{T_a}{T_s}\right) + \frac{1}{3}\left(\frac{T_a}{T_s}\right)^4 \quad (19)$$

The solar collector exergy efficiency defines the increase of fluid flow exergy upon the primary radiation exergy by the radiation source. The exergy efficiency is calculated as :

$$\eta_{ex} = \frac{\dot{m}C_p\left(\left(T_o - T_i\right) - T_a \log\left(\frac{T_o}{T_i}\right)\right)}{A_p I \eta_p} \quad (20)$$

2.2. Economic Analysis

The economic analysis allows choosing the economically feasible system. Under this heading, the optimum economic performance of these SAHs is expected to be determined based on the technical and economic.

In order to determine the annual cost (AC) of the collector per unit surface area, the different cost factors have to be calculated. This include the annual pumping cost (RC), the annual collector cost (ACC), the annual maintenance cost (MC), and the annual salvage value (ASV) [42]

$$AC = RC + ACC + MC - ASV \quad (21)$$

The annual pumping cost is calculated as, [42]

$$RC = \frac{\dot{m}\Delta P}{\rho} t_{op} CE \quad (22)$$

Where t_{op} is the operational time (300days in year and 8 hour in day), CE is the cost of electricity that was taken as $CE = 0.1 \,{}^{\$}\!/_{kWh}$, and ΔP is the pressure drop across flow channel that calculated in Eq 18.

The annual collector cost is calculated as,

$$ACC = (CRF)(CI) \quad (23)$$

Where (CRF) is the capital recovery factor and calculated as,

Where i is the interest rate and n is the collector life time and considered 0.1 and 10 years.

The capital investment (CI) included material cost, paint cost, fabrication cost and absorber cost.

The annual maintenance cost (MC) of the collector is considered to be 10 % of the annual collector cost (ACC).

The annual salvage value (ASV) is calculated as,

$$ASV = (SFF)(SV) \quad (25)$$

Where (SFF) is the salvage fund factor and calculated as,

$$SFF = \frac{i}{\left[(i+1)^n - 1\right]} \quad (26)$$

And

$$SV = 0.1(CI) \quad (27)$$

Now we can calculate AC for economic analysis.

All the parameters we need are listed in Table.3.

2.3. Multiobjective Optimization

Multi-objective optimization has been applied in many fields of science, where optimal decisions need to be taken in the presence of trade-offs between two or more conflicting objectives.

Table.2 The parameters of SAH

Glazing	Double Glass
Length of channel (c) (m)	2 ~ 3
Width to length of channel ratio (a/c)	0.3 ~ 0.5
Height to width of channel ratio (b/a)	1/12 ~ 1/8
Ambient temperature (T_a) ($^\circ K$)	290 ~ 320
Reynolds number ($\times 10^3$)	2 ~ 20
β ($^\circ$)	20 ~ 70
Intensity of solar radiation $\left({}^{w}\!/_{m^2}\right)$	400
ε_p	0.88
ε_g	0.86
Stephan boltzman (σ)	5.67×10^{-8}
Insulation thermal conductivity (k_i) $\left({}^{w}\!/_{m\,^\circ k}\right)$	2.5×10^{-2}
Insulation thickness (t_i) (m)	1×10^{-2}
transmittance-absorptance product (τα)	0.85
Sun temperature (T_s) ($^\circ K$)	4350
Wind velocity (V_w) (${}^{m}\!/_{s}$)	1.5

For a nontrivial multi-objective optimization problem, no single solution exists that simultaneously optimizes each objective. In this case, the objective function is minimizing cost of collector and maximize energy and exergy efficiency. To reach this goal, we use NSGA II algorithm in MATLAB software. For each geometry of rib-roughness, after optimization we have 200 data series with various energy and exergy efficiency and cost of collector. For find the best data, we use TOPSIS decision algorithm and weighing exergy and energy efficiency and cost of collector.

3. Results & Discussion

The equations used in this article have been adapted from other articles. To verify the results of this paper, validate these results with the results of other paper. Energy and exergy efficiency of SAH with roughened and smooth absorber plate in this article and Bisht [42] and Singh [32] papers. The validation results are shown in Tables 3-6. As can be seen in these tables the maximum error is 23.31%.

The result of energy and exergy analysis of SAH indicated in the Table.7 and Table.8.

In Figure 1, for example, the relationship between exergy efficiency and energy is shown for SAH with multi-v rib. With increasing energy efficiency, exergy efficiency decreases and vice versa. In this figure F1 axis show the energy efficiency and F2 show the exergy efficiency. In addition to these two parameters, the annual cost of the collector is also examined.

In this 2 table we can see that the most effective parameter for energy and exergy efficiency is reynolds number. Also we can find that the other parameters are almost constant. The multi-objective analysis and optimization examines energy and exergy and cost of collector together. It is the best way to find best condition for SAH.

Table3. Validation of energy efficiency of smooth SAH

No	$\Delta T.I$	η_{th}[42]	η_{th} – Recent Article	Error %
1	0.001	0.7395	0.728	1.56
2	0.004	0.6136	0.5799	5.49
3	0.006	0.6765	0.6612	2.26
4	0.007	0.4994	0.4663	6.62
5	0.008	0.634	0.6216	1.95
6	0.01	0.3944	0.3713	5.87
7	0.013	0.3006	0.2913	3.09
8	0.016	0.2185	0.2226	1.88

Table4. Validation of exergy efficiency of smooth SAH

No	P/e	Re	η_{ex}[47]	η_{ex} Recent Article	Error %
1	8	320	0.00506	0.00529	4.62
2		1065	0.00911	0.00897	1.54
3		2200	0.01086	0.01053	3.06
4		3017	0.1115	0.01072	3.85
5		5360	0.01040	0.01003	3.56
6		8044	0.00908	0.00897	1.19
7		10960	0.00770	0.00786	2
8		16100	0.00529	0.00652	23.31

Table5. Validation of energy efficiency of roughened SAH

No	$\Delta T.I$	η_{th}[42]	η_{th} – Recent Article	Error %
1	0.001	0.7580	0.7729	1.96
2	0.004	0.7167	0.7033	1.87
3	0.006	0.6765	0.6612	2.26
4	0.007	0.6586	0.6411	2.66
5	0.008	0.634	0.6216	1.95
6	0.01	0.5914	0.5791	2.07
7	0.013	0.5241	0.523	0.2
8	0.016	0.4599	0.4654	1.2

Table6. Validation of exergy efficiency of roughened SAH

No	P/e	Re	η_{ex}[47]	η_{ex} Recent Article	Error %
1	8	1067	0.01748	0.01789	2.32
2		3099	0.01917	0.01932	0.77
3		5000	0.01672	0.01691	1.11
4		6800	0.01433	0.01476	2.99
5		9318	0.01149	0.01255	9.26
6		11860	0.00893	0.01074	20.27

Table.7 Energy analysis of SAH with 4 different rib geometry on the absorber plate

Rib	parameters															η_{th} %
	β	V_w	a/c	b/a	c	T_a	Re	p/e	e/D_h	W/w	α	d/w	g/e	B_R	P_R	
Multi V Shape	70	1	0.3	1/12	2	296	20000	8.105	0.043	6.2	60	-	-	-	-	75.53
U Shape Turbulator	70	1	0.3	1/12	2	308	20000	6.667	0.043	-	-	-	-	-	-	70.93
Winglet and Wavy Grooves	70	1	0.3	1/12	2	292	20000	-	-	-	-	-	-	0.28	1	76.31
Discrete V Rib	70	1	0.3	1/12	2	293	20000	8.031	0.043	-	59	0.65	1.05	-	-	76.43

Table.8 Exergy analysis of SAH with 4 different rib geometry on the absorber plate

Rib	parameters															η_{ex} %
	β	V_w	a/c	b/a	c	T_a	Re	p/e	e/D_h	W/w	α	d/w	g/e	B_R	P_R	
Multi V Shape	70	1	0.3	1/12	2.3	290	2000	8.104	0.043	5.7	60	-	-	-	-	1.8
U Shape Turbulator	70	1	0.3	1/12	2	290	2000	6.667	0.04	-	-	-	-	-	-	1.4
Winglet and Wavy Grooves	70	1	0.3	1/12	2.91	290	2000	-	-	-	-	-	-	0.27	1.2	2.36
Discrete V Rib	70	1	0.3	1/12	2	290	2000	8.031	0.043	-	58	0.65	1.05	-	-	2.14

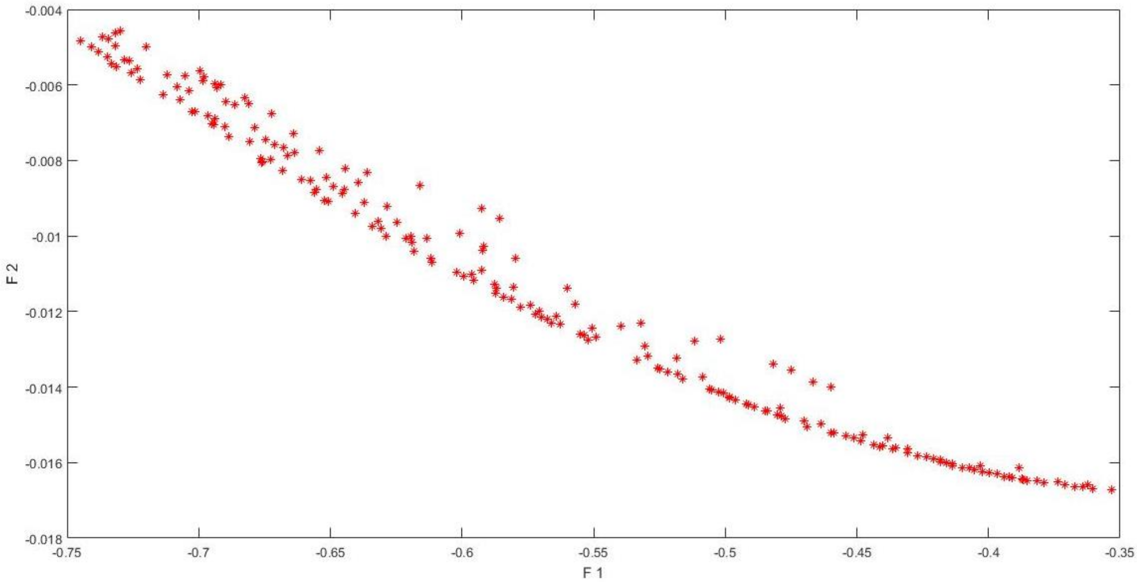

Figure.1 Relationship between exergy efficiency and energy efficiency

The result of this optimization indicated in the Table.5.

According to table.5 annual puping cost (RC) is negligible so the pressure diference in SAH with rib-roghness on its absorber plate is not a big value. In this work, when optimize data with NSGA II algorithm, it's time to use TOPSIS algorithm to find the best data for each rib-roughness geometry. For Topsis algorithm and weiging the parameters respectively we use 0.45,0.35 and -0.2 for energy efficiency,exergy efficiency and annual cost of collector. This values can vary for your condition and priority.

Also on Table.9 we can compare different rib-roughness geometry effect on perfomance of SAH. The Multi-V rib has the best exergy efficiency and the discrete-V rib has the best energy efficiency and also low annual cost. U-shape turbulator annual cost is the lowest but in comparision with discrete-V, the discrete-V rib has a better performance.

Table.9 Multiobjective optimization of SAH with four different rib-roughness geometry on the absorber plate

Rib			AC ($)				
	η_{th}	η_{ex}	AC	ACC	MC	RC	ASV
Multi V	54.64	1.27	42.94	40.51	4.05	0.01	1.56
U shape Turbulator	55.19	0.68	18.75	17.65	1.77	0.02	0.68
Winglet and Wavy grooves	57.97	0.93	67	20.23	2.02	0.42	2.43
Discrete V	58.81	1.01	22	23.74	2.37	0.04	0.78

4. Conclusions

One of the best forms of renewable energy is solar energy. In this article, we performed a multi-objective optimization to a SAH to reach the best condition of this device. Our objective for optimization is maximizing energy and exergy efficiency and minimizing annual cost of collector (AC). Also we use 4 different rib-roughnesses on absorber plate to improve the thermal performance of device. In this case of optimization, 15 parameters are considered such as wind velocity, Reynolds number, collector tilt, ambient temperature, collector dimension (length, width and height) and rib-roughness dimension.

For optimization we choose NSGA II algorithm and find 200 data series of variable parameters. Any of these data have a good performance, but to find out the best one we should use a decision algorithm. For this purpose we use TOPSIS algorithm and weiging the objective (energy and exergy efficiency and AC) and find the best performance condition for this device. We saw the result of this optimization in Table.2 to Table.5 and discuss about that. We find out that the best rib geometry for this condition is discrete-V , that has the highest energy and exergy efficiency while it has the lowest annual cost.

Our device work in iran and useful lifetime of SAH considered to be 10 year and interest rate is 0.1.

We conclude that using the rib-roughness improves the performance of the device despite the pressure drop. Also the annual pumping power is very low and negligible and the main part of annual cost is for making device like materials, colors and fabrication cost.

References

1. Kakac, S., R.K. Shah, and W. Aung, *Handbook of single-phase convective heat transfer*. 1987, United States: John Wiley and Sons Inc.
2. Prasad, K. and S.C. Mullick, *Heat transfer characteristics of a solar air heater used for drying purposes.* Applied Energy, 1983. **13**: p. 83-93.
3. Prasad, B.N. and J.S. Saini, *Effect of artificial roughness on heat transfer and friction factor in a solar air heater.* Solar Energy, 1988. **41**(6): p. 555-560.
4. Karwa, R., *Experimental Studies of Augmented Heat Transfer and Friction in Asymmetrically Heated Rectangular Ducts with Ribs on the Heated Wall in Transverse, Inclined, V-Continuous and V-Discrete Pattern.* International Communications in Heat and Mass Transfer - INT COMMUN HEAT MASS TRANS, 2003. **30**: p. 241-250.
5. Ebrahim Momin, A.-M., J.S. Saini, and S.C. Solanki, *Heat transfer and friction in solar air heater duct with V-shaped rib roughness on absorber plate.* International Journal of Heat and Mass Transfer, 2002. **45**(16): p. 3383-3396.
6. Cho, H.H., et al., *The Effects of Gap Position in Discrete Ribs on Local Heat/Mass Transfer in a Square Duct.* Journal of Enhanced Heat Transfer - J ENHANC HEAT TRANSF, 2003. **10**: p. 287-300.
7. Aharwal, K.R., B. Gandhi, and J.S. Saini, *Heat transfer and friction characteristics of solar air heater ducts having integral inclined discrete ribs on absorber plate.* International Journal of Heat and Mass Transfer - INT J HEAT MASS TRANSFER, 2009. **52**: p. 5970-5977.
8. Hans, V., R.P. Saini, and J.S. Saini, *Performance of artificially roughened solar*

air heaters—A review. Renewable and Sustainable Energy Reviews, 2009. **13**: p. 1854-1869.

9. Esen, H., et al., *Modelling of a new solar air heater through least-squares support vector machines.* Expert Systems with Applications, 2009. **36**(7): p. 10673-10682.
10. Esen, H., et al., *Artificial neural network and wavelet neural network approaches for modelling of a solar air heater.* Expert Systems with Applications, 2009. **36**(8): p. 11240-11248.
11. Ozgen, F., M. Esen, and H. Esen, *Experimental investigation of thermal performance of a double-flow solar air heater having aluminium cans.* Renewable Energy, 2009. **34**(11): p. 2391-2398.
12. D., G., *Investigations on fluid flow and heat transfer in solar air heaters with roughened absorbers.* Ph.D. thesis, University of Roorkee, 1993.
13. RP, S., *Study of enhancement of energy collection rates of solar air heaters using artificial roughness in the air ducts.* Ph.D. thesis, University of Roorkee, 1996.
14. Karwa, R., S.C. Solanki, and J.S. Saini, *Thermo-hydraulic performance of solar air heaters having integral chamfered rib roughness on absorber plates.* Energy, 2001. **26**(2): p. 161-176.
15. Karwa, R. and K. Chauhan, *Performance evaluation of solar air heaters having v-down discrete rib roughness on the absorber plate.* Energy, 2010. **35**(1): p. 398-409.
16. A, B., *Advanced engineering thermodynamics.* . Wiley Interscience Pub, 1988.
17. Lior, N. and N. Zhang, *Energy, exergy, and Second Law performance criteria.* Energy, 2007. **32**(4): p. 281-296.
18. Layek, A., J.S. Saini, and S.C. Solanki, *Second law optimization of a solar air heater having chamfered rib–groove roughness on absorber plate.* Renewable Energy, 2007. **32**(12): p. 1967-1980.
19. Gupta, M.K. and S.C. Kaushik, *Performance evaluation of solar air heater for various artificial roughness geometries based on energy, effective and exergy efficiencies.* Renewable Energy, 2009. **34**(3): p. 465-476.
20. Gupta, M.K. and S.C. Kaushik, *Performance evaluation of solar air heater having expanded metal mesh as artificial roughness on absorber plate.* International Journal of Thermal Sciences, 2009. **48**(5): p. 1007-1016.
21. Altfeld, K., W. Leiner, and M. Fiebig, *Second law optimization of flat-plate solar air heaters Part I: The concept of net exergy flow and the modeling of solar air heaters.* Solar Energy, 1988. **41**(2): p. 127-132.
22. Gupta, M.K. and S.C. Kaushik, *Exergetic performance evaluation and parametric studies of solar air heater.* Energy, 2008. **33**(11): p. 1691-1702.
23. Kurtbas, İ. and A. Durmuş, *Efficiency and exergy analysis of a new solar air heater.* Renewable Energy, 2004. **29**(9): p. 1489-1501.
24. Öztürk, H.H. and Y. Demirel, *Exergy-based performance analysis of packed-bed solar air heaters.* International Journal of Energy Research, 2004. **28**(5): p. 423-432.
25. Ucar, A. and M. Inallı, *Thermal and exergy analysis of solar air collectors with passive augmentation techniques.* International Communications in Heat and Mass Transfer, 2006. **33**(10): p. 1281-1290.
26. Esen, H., *Experimental energy and exergy analysis of a double-flow solar air heater having different obstacles on absorber plates.* Building and Environment, 2008. **43**(6): p. 1046-1054.
27. Sami, S., N. Etesami, and A. Rahimi, *Energy and exergy analysis of an indirect solar cabinet dryer based on mathematical modeling results.* Energy, 2011. **36**(5): p. 2847-2855.
28. Akbulut, A. and A. Durmuş, *Energy and exergy analyses of thin layer drying of mulberry in a forced solar dryer.* Energy, 2010. **35**(4): p. 1754-1763.
29. Midilli, A. and H. Kucuk, *Energy and exergy analyses of solar drying process of pistachio.* Energy, 2003. **28**(6): p. 539-556.
30. Kaygusuz, K. and T. Ayhan, *Exergy analysis of solar-assisted heat-pump systems for domestic heating.* Energy, 1993. **18**(10): p. 1077-1085.
31. Torres R, E., M. Picon Nuñez, and J. Cervantes de G, *Exergy analysis and*

optimization of a solar-assisted heat pump. Energy, 1998. **23**(4): p. 337-344.
32. Singh, S., S. Chander, and J.S. Saini, *Exergy based analysis of solar air heater having discrete V-down rib roughness on absorber plate.* Energy, 2012. **37**(1): p. 749-758.
33. Skullong, S., et al., *Heat transfer augmentation in a solar air heater channel with combined winglets and wavy grooves on absorber plate.* Applied Thermal Engineering, 2017. **122**: p. 268-284.
34. Hans, V.S., R.P. Saini, and J.S. Saini, *Heat transfer and friction factor correlations for a solar air heater duct roughened artificially with multiple v-ribs.* Solar Energy, 2010. **84**(6): p. 898-911.
35. Bopche, S.B. and M.S. Tandale, *Experimental investigations on heat transfer and frictional characteristics of a turbulator roughened solar air heater duct.* International Journal of Heat and Mass Transfer, 2009. **52**(11): p. 2834-2848.
36. Singh, S., S. Chander, and J.S. Saini, *Heat transfer and friction factor correlations of solar air heater ducts artificially roughened with discrete V-down ribs.* Energy, 2011. **36**(8): p. 5053-5064.
37. Varun, R.P. Saini, and S.K. Singal, *Investigation of thermal performance of solar air heater having roughness elements as a combination of inclined and transverse ribs on the absorber plate.* Renewable Energy, 2008. **33**(6): p. 1398-1405.
38. Klein, S.A., *Calculation of flat-plate collector loss coefficients.* Solar Energy, 1975. **17**: p. 79.
39. Zografos, A.I., W.A. Martin, and J.E. Sunderland, *Equations of properties as a function of temperature for seven fluids.* Computer Methods in Applied Mechanics and Engineering, 1987. **61**(2): p. 177-187.
40. Petela, R., *Exergy of Heat Radiation.* Journal of Heat Transfer, 1964. **86**(2): p. 187-192.
41. Choudhury, C., P.M. Chauhan, and H.P. Garg, *Performance and cost analysis of two-pass solar air heaters.* Heat Recovery Systems and CHP, 1995. **15**(8): p. 755-773.
42. Singh Bisht, V., A. Kumar Patil, and A. Gupta, *Review and performance evaluation of roughened solar air heaters.* Renewable and Sustainable Energy Reviews, 2018. **81**: p. 954-977.